Construction and Building Materials 28 (2012) 807–818

Contents lists available at SciVerse ScienceDirect

Construction and Building Materials

journal homepage: www.elsevier.com/locate/conbuildmat

Experimental testing of the durability of lime-based mortars used for rendering historic buildings

A. Arizzi [a,*], H. Viles [b], G. Cultrone [a]

[a] Universidad de Granada, Departamento de Mineralogía y Petrología, Campus Fuentenueva s/n, 18071 Granada, Spain
[b] School of Geography and the Environment, Centre for the Environment (Dyson Perrins Bldg.), University of Oxford, South Parks Road, Oxford OX1 3QY, United Kingdom

ARTICLE INFO

Article history:
Received 20 June 2011
Received in revised form 19 September 2011
Accepted 2 October 2011

Keywords:
Freeze–thaw
Salt capillary absorption
Salt surface deposition
Environmental scanning electron microscopy
Ion chromatography

ABSTRACT

To find out which render mortar mix shows the best durability properties, we have designed four ageing tests that aim to simulate water movements, ice formation and salt crystallization in lime mortars exposed to an extreme, but realistic, range of temperature and humidity. It has been found that the response of individual mortar mixes differs according to the mechanism and the agent of attack. These findings suggest that in order to provide useful data both the experimental testing approach and the types of mortar tested need to be tailored for the particular circumstance in which the render will be applied.

1. Introduction

Rendering mortars have always been considered the sacrificial layers of walls and building facades because their main purpose, as well as an aesthetic one, is to protect the masonry structure against weathering, slowing its decay. To ensure this function, renders need to be maintained and repaired or substituted by other compatible mortars when damaged. The major benefit achieved by covering a building with a render is the reduction of moisture present inside the masonry structure [1]. The presence of water and its movement inside the pore network of mortars are among the biggest causes of their degradation [1–3]. In fact, depending on the conditions of temperature and humidity, water in both vapour and liquid state can allow freezing–thawing phenomena, can favour the entry of salts which crystallize inside the matrix, and can cause the reduction of mortar mechanical strengths and adhesion to the masonry. As a general rule, a render should be characterised by low water absorption and high water vapour permeability, so that the water which enters the mortar can easily and quickly evaporate [4], as well as by high flexibility, good adhesion and compatibility with the support (i.e. stone, brick) [5,6]. Adequate design of the masonry materials and good knowledge of their characteristics (pore system, hygric and physic-mechanical properties) are required to predict and, consequently, minimise their decay.

Accelerated weathering tests are the easiest, quickest and most commonly used way to study the resistance of a construction material exposed to certain environmental conditions as well as to know which factors are involved in its decay and in which way the material properties are affected [7]. However, one must bear in mind that natural weathering is a combination of conditions (i.e. temperature, relative humidity, solar radiation, wind, rain, salts and pollutants) which are hard to reproduce faithfully by a laboratory test. Moreover, the layer of mortar (1–3 cm thick) applied on the surface of a wall may show different textural characteristics (such as pore systems) to a laboratory sample (the standard size is 4 × 4 × 16 cm) and consequently, it may be affected in a different way by weathering. However, the performance of accelerated ageing tests is still the most useful tool for understanding the mechanisms of decay occurring in rocks and masonry structures.

Freeze–thaw cycles, mechanical stress and salt crystallization are the most effective causes of degradation of mortar used in renders. According to some authors [8,9], decay due to freezing–thawing cycles, rainfall and salts attack is more noticeable in mortars with high porosity and low strength.

Good understanding of the growth mechanisms of salts in porous materials has been achieved by many salt crystallization tests performed during the last 20 years [9–21].

* Corresponding author. Tel.: +34 58240077; fax: +34 958243368.
E-mail address: arizzina@ugr.es (A. Arizzi).

0950-0618/$ - see front matter © 2011 Elsevier Ltd. All rights reserved.
doi:10.1016/j.conbuildmat.2011.10.059

In mortars, sulphate attack consists of a sequence of three sub-processes: firstly, sulphate ions diffuse into the pores of the mortar, more or less easily depending on its permeability; secondly, the sulphate ions react with calcium hydroxide, thus enhancing further penetration of sulphates into the matrix; finally, gypsum or ettringite precipitates, depending on the composition of the binder (lime or cement) [21]. Gypsum and ettringite are responsible for the development of cracks and spalling, respectively [9]. In cement mortars, further deterioration is due to the degradation of calcium silicate hydrates with consequent leaching of calcium hydroxide [9]. The presence of thaumasite, which is similar to ettringite but derives from the reaction between calcium silicate hydrates and sulphate ions, has also been reported in cement, lime and gypsum-based mortars [22,23].

Magnesium (epsomite and hexahydrite) and sodium (thenardite and mirabilite) sulphates are the most dangerous salts for building material durability, because they normally crystallize inside the material [24] often only a few millimetres below the surface, depending on the salt viscosity and the drying rate of the material [25]. Due to their high crystallization pressure [26], these salts cause cracks, sanding and spalling.

Karatasios et al. [11] described the degradation of calcitic lime mortars due to sodium sulphate crystallization and demonstrated how the addition of barium hydroxide enhances the resistance to salts, by blocking Ca^{2+} dissolution and further precipitation of salts. The use of industrial residues (such as blast furnace slag) as additives in mortars has proved to be effective in reducing the damage caused by salt crystallization and freezing–thawing cycles [27].

The objective of this work is to study the durability of lime-based mortars to be used as rendering materials in restoration interventions. To study the effect of ageing on the properties of these mortars, they have been subjected to accelerated weathering, by simulating the extreme atmospheric conditions (of temperature and relative humidity) which occur during 1 year in the city of Granada (Andalusia, South of Spain) (Table 1).

The damage caused by rain and freezing–thawing cycles has also been studied by simulating rainfall (that mostly occurs in winter time in Granada).

Two further tests have also been carried out to study the impact of salt crystallization on mortars: the salt solution was applied during the weathering cycles as a "salt fog" on the surface of mortars, whilst other samples were placed in contact with a combination of sand and salt and periodically activated by water. In the first case, previous studies have found that fog enhances stone decay by salt because it is a source of moisture [20] and it controls the rate of breakdown, whilst salt controls timing [17]. In the second case, simulations of hyper-arid environments (such as deserts) previously performed on stone samples have demonstrated that salt weathering can operate quickly on samples not fully immersed in saline solutions but in contact with a combination of salt and sand [20].

The effect of these four weathering cycles on mortar samples has been monitored by means of visual and photographic observations, as well as by using weight loss and microscopic techniques.

1.1. Atmospheric conditions of the city of Granada (Andalucía, Spain)

Granada is located at the foot of Sierra Nevada Mountains in Spain at an elevation of 738 m above the sea level and at a distance of 60 km from the Mediterranean coast. Due to this particular geographic location, the city is characterised by extremely hot summers, during which temperatures can reach 40 °C (and about 50 °C in the sun), and quite cold winters when temperatures sometimes fall below 0 °C (see Table 1). Moreover, a temperature range of 30 °C can be registered between night and day.

Granada is one of the most polluted cities of Spain, especially because of the high amount of particulate matter produced by traffic. The amount of PM_1, PM_{10}, and NO_2, recorded in 2009 and 2010 in many areas of the city [28,29], was higher than the legal limit. On the other hand, the lowest values of contamination were registered for SO_2 and CO gas in 2009 [28]. However, the accelerating effects of suspended particles on mortar decay caused by the interaction with SO_2 gas and the formation of deleterious sulphate salts should be taken into account [30–33]. The main sources of sulphate ions which give rise to these salts are thought to be traffic and industries, as only a small portion of SO_4^{2-} ion incorporated into the atmospheric aerosol originates in sea spray [34]. Moreover, the most deleterious damage found in stones and composite materials of ancient buildings of Granada has been caused by the crystallization of magnesium salts [35,36]. Sulphate and magnesium ions are likely to come from the soil (ground water) and/or from adjacent lime or gypsum mortars, often prepared with dolomitic aggregates because dolostones commonly outcrop near Granada. In modern repair works, dolomitic lime and aggregate have been substituted by calcite due to the harmful effect of magnesium ions [24–26,30]. However, the high abundance of these elements is still a big cause of deterioration of the materials present in the historic buildings of Granada [36].

2. Materials and methods

The following components were used in the production of the test mortars: a calcitic dry hydrated lime (CL90-S [37]) produced by ANCASA (Seville, Spain), a calcareous aggregate (CA) with a continuous grading from 0.063 to 1.5 mm, a pozzolan (CLASS N POZZOLAN, [38]), produced by Burgess Pigment Company (USA) as additive, and three different admixtures: a lightweight aggregate (perlite), a water-retaining agent (cellulose derivative) and a plasticiser (polycarboxylate) (additional detail can be found at www.argosdc.com). Four types of lime mortars were prepared, in which the binder-to-aggregate (B/S) ratios were 1:3, 1:4, 1:6 and 1:9 by weight, whilst the pozzolan was kept at 10% of the total binder (by mass) and the total admixtures proportion was less than 2% of the total mass, as shown in Table 2. The mortars have been labelled M3, M4, M6, M9, according to their B/S ratio. Mortars were stored for 7 days in normalised steel moulds (4 × 4 × 16 cm) at

Table 1
Atmospheric conditions occurred in Granada in 2009. Data were taken from the Meteorological station 84,190 (LEGR) of Granada Airport (latitude: 37.18°; longitude: −3.78°; altitude: 567 m). The most extreme conditions were registered in July and January.

Year 2009	T_{max} (C)/average	T_{min} (C)/average	HR_{max} (%)/average
January	15/10	−6/1	99/87.9
February	19.3/14.4	−3/1.5	90/77.3
March	24/18.7	−0.2/4.5	97/71.3
April	24.8/18.6	−1.8/4.2	85/64.7
May	34/27	3.6/9.3	67/52.2
June	38/31.8	9.4/14.5	70/45.5
July	39.7/35.8	11.7/16	47/37.3
August	37/34.4	11.3/15.6	57/46.1
September	35.7/27.3	7.5/12.8	90/65.1
October	32.8/26.3	5.5/9.2	85/64.4
November	27/19	−0.7/4.3	96/69.3
December	19.4/13.8	−4.1/3	95/85.4

Table 2
Proportions (expressed in g) of components used in the elaboration of the four mortar types. Abbreviations indicate: calcitic lime (CL); metakaolin (MK); calcareous aggregate (CA); admixtures (perlite + cellulose derivative + polycarboxylate).

Mortars name	Components name and proportions			
	CL	MK	CA	admixtures
M3	450.0	50.0	1500.0	34.0
M4	360.0	40.0	1600.0	34.0
M6	257.1	28.6	1714.3	34.0
M9	180.0	20.0	1800.0	34.0

RH = 60 ± 5% and T = 20 ± 5 °C following a modification of the standard UNE-EN 1015-2 [39] proposed by Cazalla [40]. After being removed from the moulds, they were cured at the same conditions of T and RH until the beginning of the study. The weathering experiments were carried out three months later in order to ensure good carbonation, because the standard time of 28 days was considered too short for ensuring carbonation and properties improvement on these materials. Four different tests were performed: (1) weathering cycles with T, light and RH variations (WS); (2) weathering cycles and rain simulation (WS + R); (3) weathering cycles and salt resistance by capillary absorption (WS + SS); and (4) weathering cycles and salt resistance by surface deposition (WS + SD). Samples were weighed and photos taken every day in order to record any morphological change in mortars.

2.1. Weathering study (WS)

To study the effect of ageing process on mortar properties, the four different types of mortar were subjected to accelerated weathering, by simulating the atmospheric conditions which occur during one year in the city of Granada (Table 1). In this simulation the annual temperature and relative humidity range was repeated every 12 h. The simulation was carried out on three samples per mortar type, in a Sanyo-FE 300H/MP/R20 environmental cabinet (internal dimensions of 675 W 630D 650H mm) (School of Geography and the Environment, Oxford University, UK) which can operate at temperature range of −20 to +100 °C and can be programmed with different conditions of temperature, relative humidity and light. Three samples (each of 2 × 4 × 4 cm) per mortar were placed on a sand layer (ca. 4 cm thick) in a tray, in the same way as in Goudie et al. [17] and Goudie and Parker [20]. The smaller surface (2 × 4 cm) was put in contact with the sand and the larger surface (4 × 4 cm) perpendicular to it. In this way, samples reproduce the real situation of a render (1–3 cm thick) on a wall.

Thirty cycles were performed in total. Each climatic cycle lasted 12 h, and consisted of four steps, of 3 h duration each step, with a cooling and warming rate of 25 °C/h, as shown in Table 3. Temperature and relative humidity trends were checked with a data logger (ibutton® Hygrolog which records temperature and RH) to ensure that the programmed cycle was reproduced accurately.

2.1.1. Weathering study and rain simulation (WS+R)

Under the same weathering conditions (of T, RH and light) described in Section 2.1, rain was simulated by spraying both the sand (water level of 2 mm) and the mortar surface with around 25 mL of tap water, which was applied every four cycles just before the step at −10 °C (Table 3). The water absorbed by the samples (by capillary rise from the sand and by absorption from the wetted surface) froze when temperature decreased below 0 °C and dried when temperature increases up to 40 °C, with the consequence that freeze–thaw cycles were also simulated in this test. Thirty cycles were performed in total.

2.2. Salt resistance tests

As in most of the accelerated decay tests performed on mortars [9,11,14,21] and as recommended in standards regarding the estimation of the durability of building materials [41,42], a sodium sulphate solution was used instead of a magnesium sulphate or a sodium chloride one. In fact, if Cl^- ions accumulation decreases with the increase of the distance from the sea [34], chlorides should be scarce in Granada, although an influx of marine particles can be expected when the wind direction is southerly [36]. Moreover, the damage caused by Cl^- salts is less noticeable than the deterioration by thenardite and mirabilite, because halite always crystallizes at the material surface (as efflorescences) [10,24].

2.2.1. Weathering study and salt attack by capillary absorption (WS+SS)

The experimental design proposed by Goudie et al. [17] was used, with some modifications, to evaluate the damage caused by the capillary uptake of a saline ground water within the mortar. Samples were placed on sand 4 cm thick, in which sodium sulphate was dispersed. Among the different conditions of weathering established by Goudie et al. [17], we chose the 1:10 salt to sand ratio by weight and a water level of 1 mm applied in each tray, in order to produce observable breakdown. Ten cycles were performed in total. Tap water was applied over the tray for around 60 s, using a spray every four cycles before the step at the highest temperature (40 °C, Table 3). Ion chromatography analysis (Dionex IC DX500) (School of Geography and the Environment, Oxford, UK) was performed on mortar samples before and after the salt resistance tests, in order to determine and quantify the concentration of soluble ions.

2.2.2. Weathering study and salt attack by surface deposition (WS+SD)

To analyse the damage caused by the deposition of a salt fog on the mortar surface, a sodium sulphate solution (14% w/w) was sprayed on the surface of the mortar samples, every two cycles before the step at the highest temperature (40 °C, Table 3). Thirty cycles were performed in total. Also after the WS + SD test, ion chromatography analysis (Dionex IC DX500) was performed on mortar samples.

2.3. Carbonation degree and porosity of the mortar samples

Carbonation degree and open porosity of both internal and external zones of mortar samples were determined before and after the weathering study.

The mineralogical phases and the degree of carbonation were determined by X-ray diffraction (XRD), by means of a Panalytical X'Pert PRO MPD diffractometer (Dept. of Mineralogy and Petrology, University of Granada, Spain), with automatic loader and ŔCelerator detector, 4–70° 2θ explored area. The interpretation and quantification of the mineral phases was performed using the X-Powder software package [43]. The decrease in portlandite content was taken as a reference to estimate the carbonation degree index (I_{CD}, expressed in %), according to the equation:

$$I_{CD} = \frac{CH_0 - CH_x}{CH_0} \times 100 \quad (1)$$

where CH_x is the amount of portlandite at time x and CH_0 is the initial content of portlandite (at time 0), determined by XRD. This method of quantification is not totally accurate since it does not take in account the small amount of portlandite consumed during the hydration of metakaolin phases. For this reason I_{CD} is considered as an approximate estimation of the carbonation degree of mortars.

Open porosity (P_o, %) and pore size distribution (PSD, in a range of $0.002 < r < 200$ μm), were determined using a Micrometics Autopore III 9410 porosimeter (mercury injection porosimetry, MIP) (Dept. of Mineralogy and Petrology, University of Granada, Spain). Mortar fragments of ca. 2 cm^3 were oven-dried for 24 h at 60 °C before the analysis.

2.4. Micro-scale crystallization cycles

Environmental scanning electron microscopy (ESEM) (Scientific Instrumentation Center, Granada, Spain) allows the detailed observation of the crystalline phases of a salt at different degree of hydration. A Philips Quanta 400 was used to analyse small mortar fragments (~2 mm^3), which did not need to be previously dried and sputter coated. Before observation, the microscope chamber was purged at a temperature of 10 °C and a range of pressures between 0.9 and 5 torr, corresponding at this temperature to about 8% and 40% of relative humidity. Once equilibrium was achieved, temperature and pressure were fixed at 2 °C and 2.5 torr (RH ~ 36%), respectively. These conditions were established for the observation of the anhydrous phases in mortar samples. A low temperature ensures good working conditions and reliable results. Hydration and dehydration cycles of the salt crystals were performed with a fixed temperature of 2 °C and a range of pressure of 2–6 torr, which reproduces relative humidities of 29–87%. Three cycles were performed in total. Chemical analyses were performed by means of an EDX microanalysis system, with Si(Li) detector of SUTW type.

3. Results and discussion

The response of mortars (i.e. mass variation, deterioration forms and decay speed) to the weathering cycles was different depending on the type of attack produced in the four experimental runs by temperature and humidity changes, alternation of wet and dry

Table 3
Scheme of the exposure conditions used in the tests, which represents one cycle of 12 h duration, as indicated by the initial (T_{init}, in hours) and final (T_{fin}, in hours) time of each step. Temperature (T, in °C), relative humidity (RH, in%) and light (40 W Crompton reflector lamp) are the conditions used in all tests. "Yes" and "not" refers in which step the light was applied; "–" indicates that the relative humidity was not programmable in this step. WS: weathering study; WS + R: weathering study and rain simulation; WS + SS: weathering study and salt resistance by capillary absorption; WS + SD: weathering study and salt resistance by surface deposition. "-" indicates that no additional conditions were applied in this step.

T_{init} (h:min)	T_{fin} (h:min)	T (°C)	RH (%)	Light	WS	WS + R	WS + SD	WS + SS
00:00	03:00	40	40	yes	-	-	-	-
03:00	06:00	15	70	not	-	water spraying	-	-
06:00	09:00	−10	–	not	-	-	-	-
09:00	12:00	15	70	not	-	-	water spraying	Sodium sulphate solution spraying

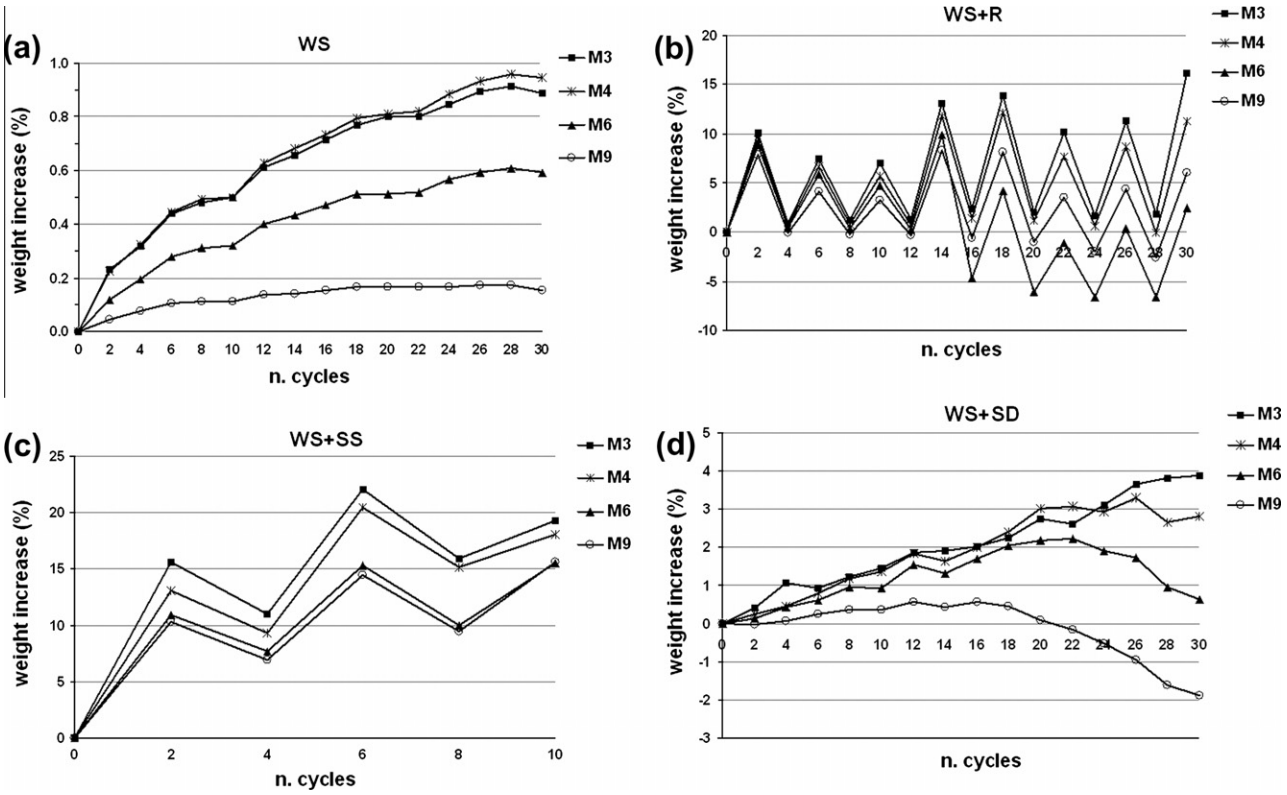

Fig. 1. Representation of the weight variations (in %) as a function of the number of cycles of the following tests: WS (weathering study) (a); WS + R (weathering study and rain simulation) (b); WS + SS (weathering study and salt resistance by capillary absorption) (c); WS + SD (weathering study and salt resistance by surface deposition) (d).

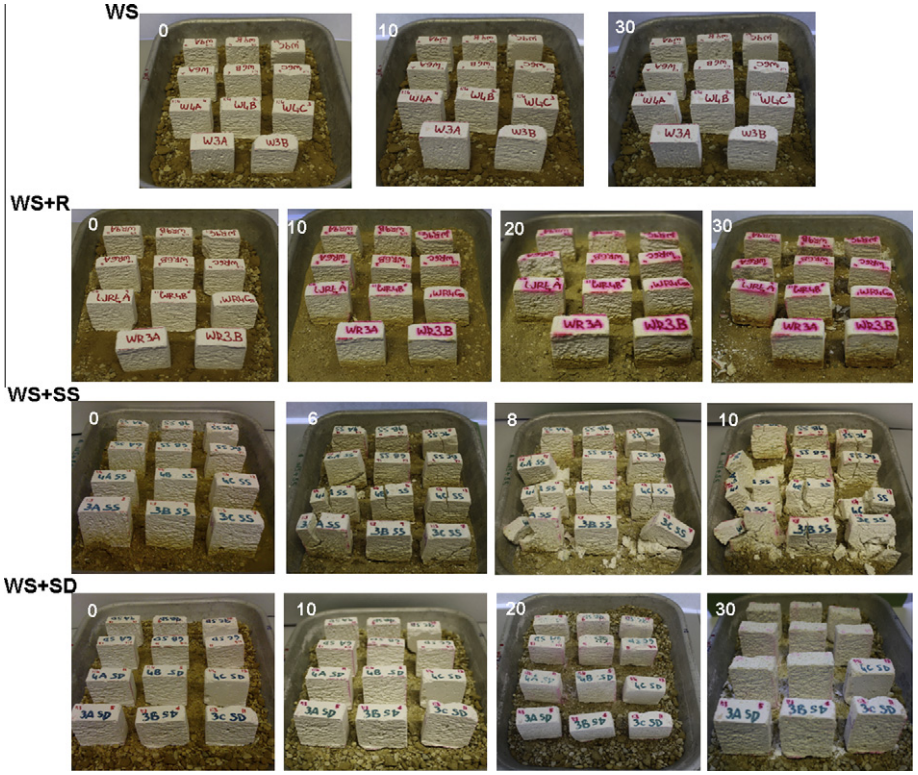

Fig. 2. Samples aspect at the beginning and during the tests. (WS): normal weathering; (WS + R): weathering study and rain simulation; (WS + SS): weathering study and salt resistance by capillary absorption; (WS + SD): weathering study and salt resistance by surface deposition. The cycle number is indicated on each image.

Table 4
Deterioration forms observed in mortars during the following tests: WS + R (weathering study and rain simulation); WS + SS (weathering study and salt resistance by capillary absorption) and the WS + SD (weathering study and salt resistance by surface deposition). The indexes used represent the number of samples (*i*: one; *ii*: two; *iii*: three) of each mortar showing the corresponding deterioration form and the number of cycles after which the deterioration form appears.

Deterioration forms	M3	M4	M6	M9
After WS + R	Mortars name			
Fissures	*i*, 30	*i*, 26	*i*, 10/*ii*, 26	*i*, 30
Fragments loss	–	*i*, 20/*ii*, 30	*i*, 14/*iii*, 20	*iii*, 20
[a]Sanding	*i*, 26/*ii*, 30	*i*, 20/*ii*, 26	*i*, 20/*iii*, 30	*iii*, 20
[b]Spalling	*i*, 26	*ii*, 26	–	–
After WS + SS	Mortars name			
Fissures	*i*, 2/*ii*, 4	*ii*, 2	*i*, 6	*i*, 2
Efflorescences	*i*, 4	*i*, 6	*i*, 6	–
Spalling	*i*, 6	–	–	–
Cracks	*iii*, 6	*iii*, 6	*ii*, 6	*ii*, 6
Fragments loss	*iii*, 8	*i*, 6	*ii*, 6/*iii*, 8	*iii*, 10
Samples breaking	*ii*, 8/*iii*, 10	*i*, 8/*iii*, 10	*i*, 8/*iii*, 10	*iii*, 10
Sanding	*iii*, 10	*iii*, 10	*iii*, 10	*iii*, 10
After WS + SD	Mortars name			
Efflorescences	*ii*, 18/*iii*, 30	*ii*, 18/*iii*, 30	*iii*, 18	*ii*, 18
Spalling	*iii*, 30	*ii*, 20/*iii*, 30	*iii*, 20	*ii*, 20
Cohesion loss and sanding	*i*, 30	*i*, 20/*ii*, 30	*ii*, 20/*iii*, 30	*iii*, 20

[a] Sanding refers to the loss of material in form of powder from the sample surfaces.
[b] Spalling refers to the detachment of layers from the sample surfaces.

periods and presence of salts. The climatic cycles reproduced by the environmental cabinet were monitored to ensure reproducibility during each test. Sample weights are shown in Fig. 1 as a function of cycle number. Changes in mortar appearance observed during the weathering cycles are shown in Fig. 2. An accurate description of the different deterioration forms developed in mortar samples during WS + R, WS + SS and WS + SD is given in Table 4 and the most representative images of those are shown in Figs. 3–5, respectively. Finally, the soluble ion content (anions, as SO_4^{2-}, and cations, as Na^+ and Ca^{2+}) determined on the mortar samples before and after the WS + SS and WS + SD tests is given in Fig. 6. In the following sections, we present a detailed description of the results obtained in each test.

3.1. WS

All mortars samples presented a slow and constant increase in weight during the WS test (Fig. 1a), especially M3 and M4, where the final weight is about a 1% higher than the initial one (Fig. 1a). On the other hand, the lowest weight increase has been registered in M9, of only +0.1%.

This fact may indicate that the mortar samples are still undergoing carbonation under these conditions, since carbonation produces a weight increase in mortars [44], and this is clearly higher in mortars with higher amount of lime. Before the weathering study, the mortars presented different carbonation degree indexes (Table 5), with higher values in M3 and M4. After WS, M4 was still the most carbonated mortar and this may explain the biggest increase in weight registered in this mortar at the end of the weathering cycles. Notwithstanding, this correspondence between weight increase and carbonation degree is not found in M3. In fact, the amount of portlandite found in this mortar after WS is the highest and this results in the lowest carbonation degree index

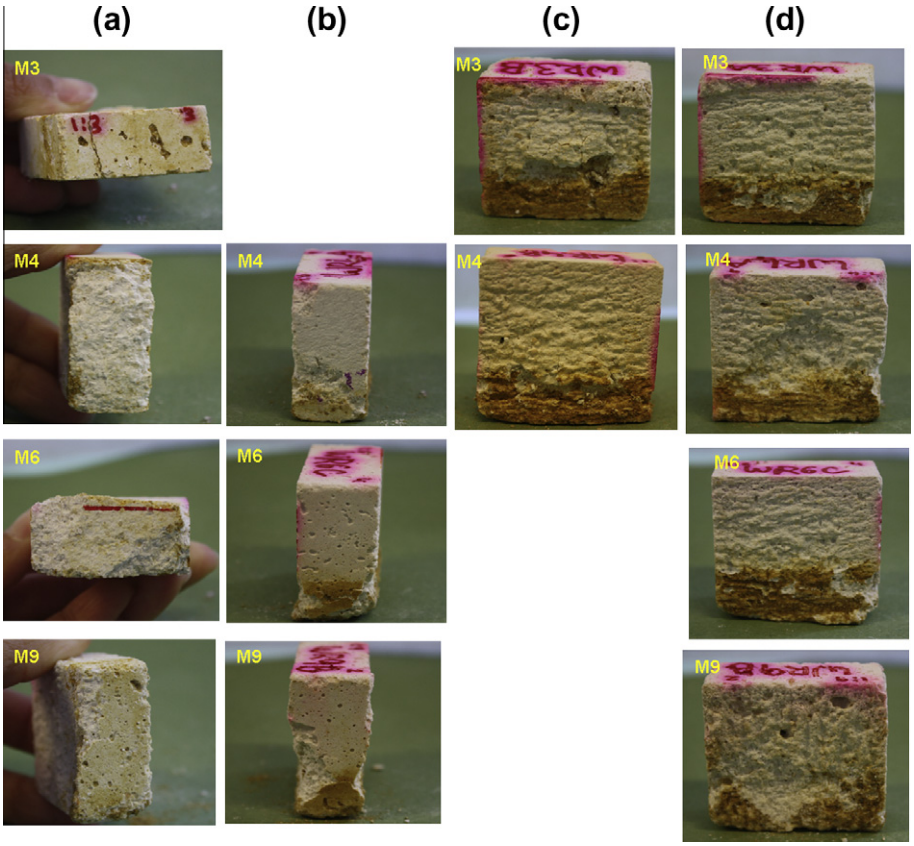

Fig. 3. Images of the different deterioration forms appeared in the mortars samples submitted to the WS + R test (weathering study and rain simulation): Fissures and fragment loss in the bottom (a) and the side (b) surfaces at the end of test; (c) spalling on the bigger surface, developed only in M3 and M4 samples after 30 and 26 cycles, respectively; (d) sanding on the bigger surface of samples at the end of the test.

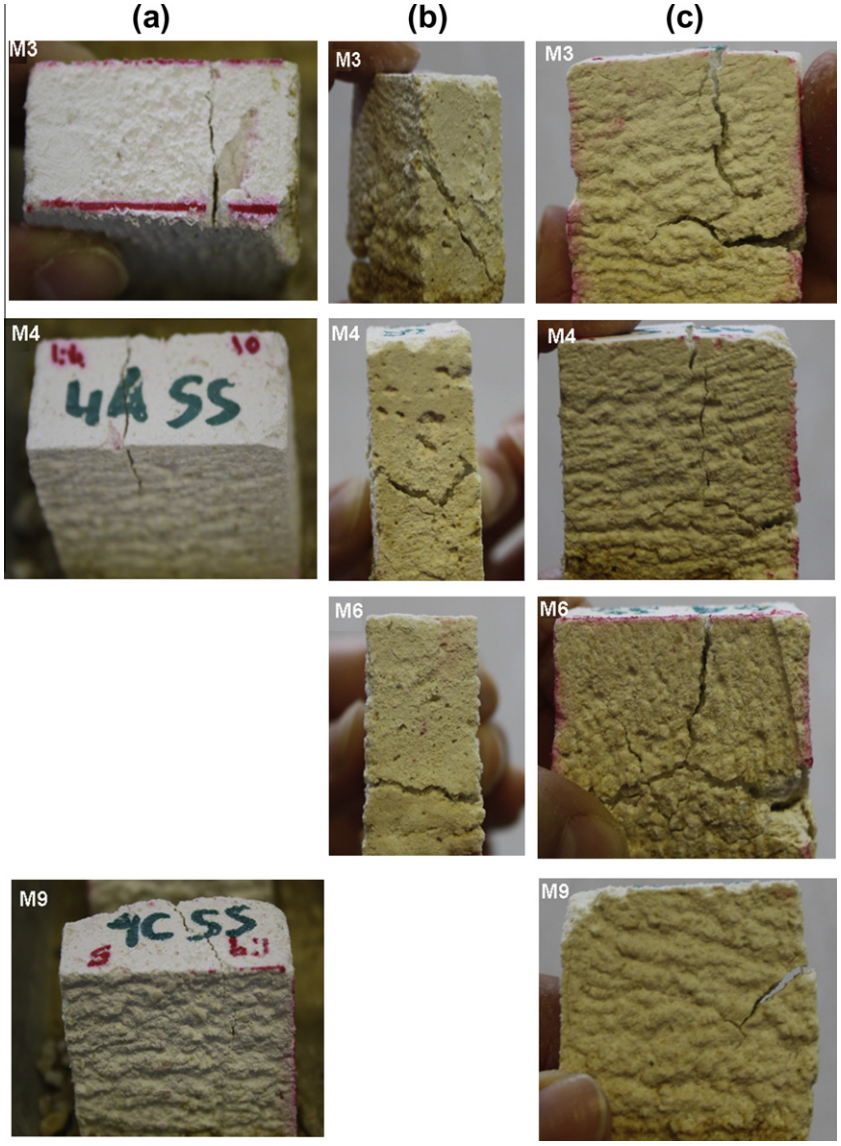

Fig. 4. Images of the different deterioration forms appeared in the mortars samples submitted to the WS + SS test (weathering study and salt resistance by capillary absorption): (a) Fissures developed after four cycles in samples M3, M4 and M9. (b) Efflorescences appeared after six cycles on the side surfaces of samples M3, M4 and M6; spalling also appears on sample M9. (c) Fractures in form of cross developed in all samples after six cycles.

at the end of the test. On the other hand, the weight of M3 samples recorded after 30 cycles of WS is one of the highest (Fig. 1a). This discrepancy can be explained by considering the differences found in the X-ray diffraction patterns of M3 and M4 (Fig. 7). In both patterns, calcite and portlandite are present but in M3 about 5% of the total amount of mineral phases is represented by the CAĈH phase ($Ca_4Al_2(CO_3)(OH)_{12}\cdot 6H_2O$, or monocarboalluminate). As shown in Fig. 7, the amount of this phase is the highest in M3 mortar. The CAĈH is one of the mono-phase calcium hydrates (AFm) that derives from the reaction between the reactive alluminates of metakaolin and the CO_3^{2-} ions [45]. According to Cizer [46], this monocarboalluminate replaces progressively its precursor (hemicarboaluminate) in the presence of excess calcite and this leads to the liberation of calcium hydroxide (i.e., portlandite) and thus to an increase in its amount. If 5% of CAĈH has been formed in M3 after the WS cycles, it is likely that calcium hydroxide is liberated during CAĈH formation and precipitates as portlandite, with the consequence that the amount of this phase is higher than expected. On this basis and according to the higher weight increase registered in M3 after WS, we can believe that M3 is still one of the most carbonated mortars at the end of this test.

Calcium silicate hydrates (CSH) and calcium alumina silicate hydrate (CASH) detected in some of the samples (Fig. 7) are among the major phases formed after pozzolanic reaction of the metakaolin [46].

Mortar samples did not show any visible change (i.e. deterioration) during the WS cycles, as shown in Fig. 2a. The only modification was found at microscopic scale and concerns the pore size distribution of mortar samples (Fig. 8a). In the unaltered samples, the main peak obtained in the PSD curves corresponds to pores with radii between 0.1 and 1 μm and whose volume is the most influential on the open porosity of mortars (P_o, Table 5). Another range of smaller pores ($0.01 < r < 0.04$ μm) is present in the unaltered samples and their volume is bigger in M3 and M4, which were prepared with a higher content of binder (i.e. lime + metakaolin). After the WS test, M3, M4 and M6 show a decrease in the amount of pores in the main range ($0.1 < r < 1$ μm). Since MIP analysis only detects interconnected pores, the volume reduction of

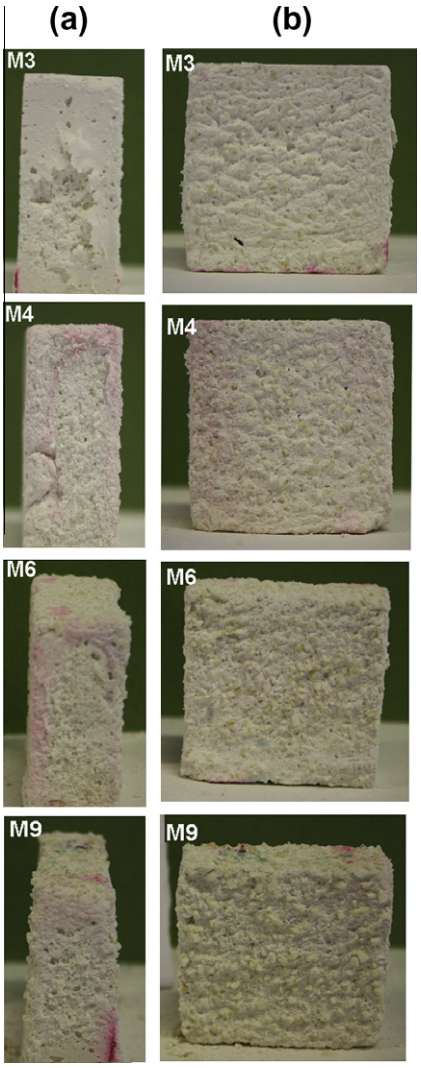

Fig. 5. Images of the different deterioration forms appeared in the mortars samples submitted to the WS + SD test (weathering study and salt resistance by surface deposition). (a) Efflorescences and spalling observed on the side surfaces of the same samples, at the end of the test. (b) Surface aspect of the different mortars samples at the end of the test.

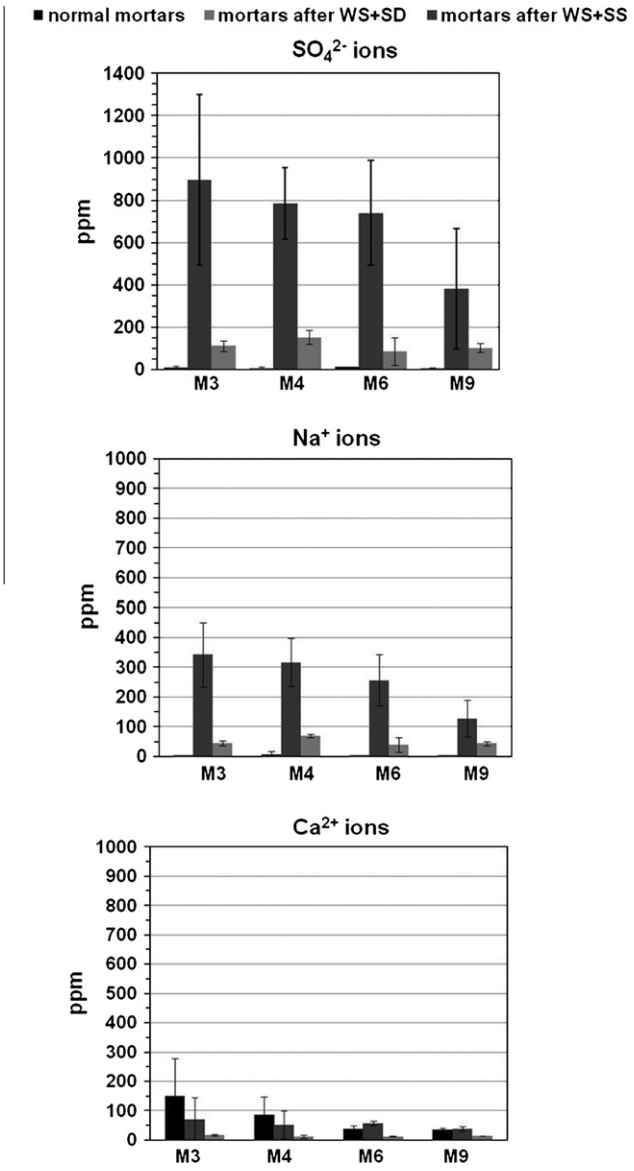

Fig. 6. Soluble ions (sulphates, SO_4^{2-}; sodium, Na^+; calcium, Ca^{2+}) concentration (in ppm) determined on M3, M4, M6 and M9 samples before (normal mortars) and after the WS + SS (weathering study and salt resistance by capillary absorption) and WS + SD (weathering study and salt resistance by surface deposition) tests. Error bars represent the standard deviation determined on three samples per mortar.

pores of the same size indicates that the interconnection among these pores decreases. This occurs due to calcite crystallization during the carbonation process [47].

3.2. WS + R

In this test, besides the moisture uptake in mortars caused by the alternation of wet and dry periods, decay is also driven by the formation of ice inside them when temperature goes below 0 °C (see Section 2.1). Fig. 1b shows the influence of this alternation of wet and dry periods on the weight of samples: a weight increase (between 5% and 14%) was registered two cycles after the water application (i.e. simulation of rain fall). At the end of the test, the only increase in final weight was recorded in M3 samples (by about 2%) whilst M4 samples recovered their initial weight and M6 and M9 samples lost weight. These differences in sample weight as well as the changes observed in the appearance of samples during the WS + R test (Fig. 1b) indicate that the application of water, both on the sand and the surface of the samples, produced a much more pronounced response than the temperature and relative humidity cycles alone and that this response is different according to the mortar type.

The most rapid deterioration was observed in M6, where in one sample the development of a long fissure led after a few cycles to the detachment of a large fragment parallel to the surface (Table 4). The consequent mass loss suffered by this sample is responsible for the great decrease in weight registered for M6 at the end of the test (Fig. 1). However, given that this decay only occurred in one sample, it is likely to be initiated to a stress produced when the sample was cut before the test instead of being driven entirely by the test conditions.

In M4 and M6 the development of fissures on the bottom face of the samples led to the loss of small fragments from the same surface, whilst in M9 no fissures were detected before the loss of fragments (Table 4 and Fig. 3a). M3 did not show any loss of fragments unlike the other samples, but the development of a fissure in the bottom face of one of the M3 samples (Table 4 and Fig. 3a) after 30 cycles, allows us to expect a similar decay for this mortar, even

Table 5
Carbonation degree index (I_{CD}, in %, measured according to Eq. (1)) and open porosity (P_o, in %) of mortars before (unaltered) and after the different weathering processes: WS (weathering study); WS + R (weathering study and rain simulation); WS + SS (weathering study and salt resistance by capillary absorption) and the WS + SD (weathering study and salt resistance by surface deposition).

Mortar name	I_{CD} (%)		P_o (%)				
	Unaltered	After WS	Unaltered	After WS	After WS + R	After WS + SS	After WS + SD
M3	33	55	38.9 ± 5.0	36.3 ± 2.0	36.2 ± 4.0	38.5 ± 0.3	37.5 ± 0.7
M4	34	85	34.5 ± 0.2	34.1 ± 0.4	35.4 ± 1.1	42.0 ± 5.0	32.9 ± 0.3
M6	28	75	31.8 ± 0.2	32.0 ± 0.1	32.7 ± 1.0	38.2 ± 5.6	30.2 ± 1.3
M9	30	65	31.3 ± 0.9	32.5 ± 0.1	33.1 ± 0.5	37.1 ± 2.0	30.0 ± 0.8

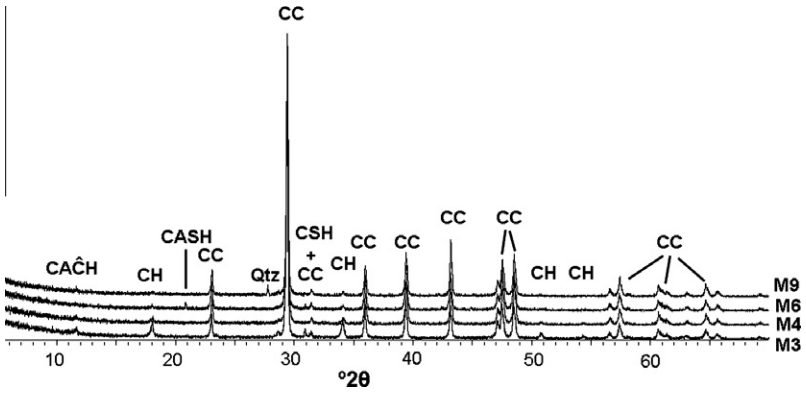

Fig. 7. XRD pattern of mortars after the weathering study (WS). CC: calcite; CH: portlandite; CAĈH: monocarboalluminate; CSH: calcium silicate hydrate; CASH: calcium alumina silicate hydrate; Qtz: quartz.

if slower. The loss of small fragments also occurred from the side surfaces of samples M4, M6 and M9 but later than from the bottom (Fig. 3b). This deterioration form (i.e. loss of fragments) was observed only on the surfaces in direct contact with water.

The decay of the bigger surface of samples differed according to the mortar type. In M3 and M4 spalling occurred first (Table 4) and, after the total detachment and fall of the superficial layers due to the volume increase (9%) caused by the ice formation, the surface below, already damaged by the previous process, was furthermore exposed to the water sprayed on the surface, which formed a film that froze and deteriorated the sample surface, with the consequence that sanding appeared (Fig. 3c and d). On the other hand, spalling did not occur in any samples of M6 and M9 and sanding directly occurred on the bigger surface (Table 4 and Fig. 3d), suggesting that in this case the most aggressive agent was the frozen water present on the surface of these mortars.

Surface flaking and internal damage are the two types of cracking recognised in mortars subjected to freezing–thawing phenomena in previous studies [48].

To explain the observed differences in the modifications of samples' appearance it is useful to study the modifications of the pore system of the mortars after the WS + R test. In M3 and M4 PSD curves, the main peak is shifted to smaller pore radius and the volume of these pores is lower (Fig. 8a). Moreover, the volume of pores with radius lower than 0.1 μm increases slightly. This indicates that water freezing has caused a shift of the maximum peak, with a smaller radius than the original one. The water movements within the mortar are responsible for the precipitation of calcite in the pores, as well as for the rearrangement of phases in the matrix system, which cause the observed pore network. At the same time, few pores with radius around 4 μm appear. This is probably due to a partial destruction of the pore system caused by freeze–thaw mechanism. On the other hand, in M6 and M9 the only change found in the PSD curves is the volume reduction or increase of the original pores. Particularly, the increase of the pore volume obtained in M9 is caused by the bad cohesion existing between matrix and aggregate grains that characterises mortars with high aggregate contents [49].

3.3. Salt resistance tests

3.3.1. WS + SS

Here, the mechanism of attack consists in the salt dissolution in water and in the following absorption of the salty solution by capillary rise. Due to the weathering cycles to which the samples are submitted in the meantime, the sulphate undergoes cycles of precipitation (at higher T) and dissolution (at lower T) processes inside the samples, leading to observable decay, which occurred after 10 cycles.

The WS + SS weight curves shown in Fig. 1c present the alternation of positive and negative peaks (as obtained in the WS + R test, Fig. 1b) which indicates how sensitive the weight of mortar samples is to the activation of the salt with water, which was performed every four cycles. About 5% of weight is lost between a wet and a dry cycle but more than 10% of weight is gained after the salt activation, with the consequence that the combined action of wet/dry periods and salt results in a general weight increase in all mortar samples. At the end of the test, M3 samples showed the biggest weight increase (almost 20%), followed by M4 which recorded a weight increase only 1% lower than M3. M6 and M9 behaved in a very similar way, with the same final increase in weight, equal to 15%. The weight increase is related to salt uptake by the mortar. However, the final weight recorded is lower than expected because of the many fragments lost at the end of the test which could not be weighed, because they were very fragile and reduced to powdered fragments after being handled (Fig. 2c).

During the WS + SS test, the first deterioration form that appeared in mortars was the formation of fissures which developed perpendicularly to the upper face and along the bigger face of the samples (Table 4 and Fig. 4a). This deterioration was followed

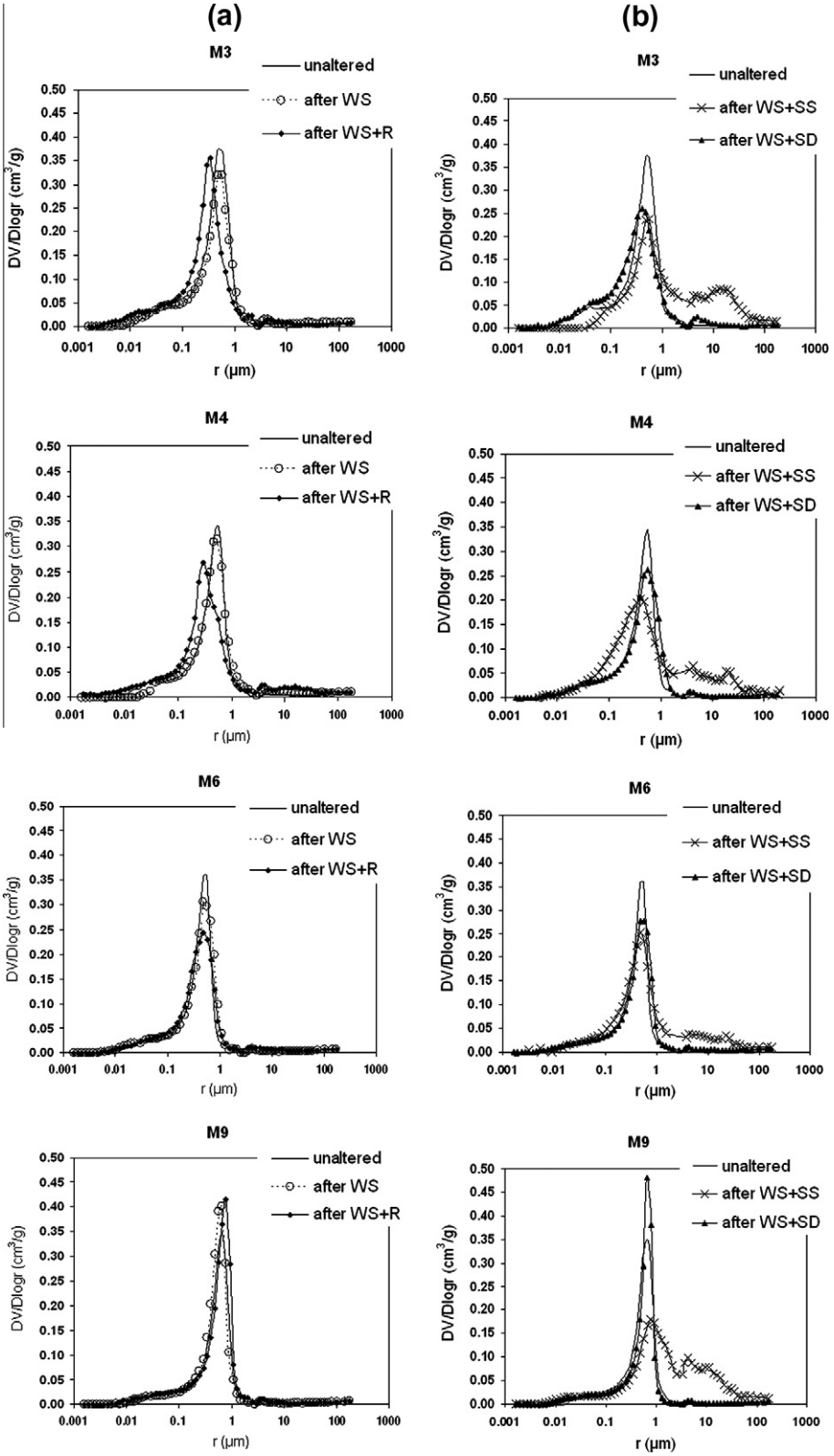

Fig. 8. Pore size distribution curves of mortars samples before (unaltered) and after the different weathering processes: WS (weathering study); WS + R (weathering study and rain simulation); WS + SS (weathering study and salt resistance by capillary absorption) and the WS + SD (weathering study and salt resistance by surface deposition).

by the precipitation of sulphate on the side faces of the samples. In some cases, the salt precipitated on the surface in the form of efflorescences and in other cases as subflorescences, very close to the surface, causing the detachment of thin layers (i.e. spalling) (Table 4 and Fig. 4b). As the test continued, fissures spread and widened until they became large cracks in the form of a cross on the bigger face, already evident after six cycles (Table 4 and Fig. 4c). These cracks caused the total breaking of the samples after 10 cycles (Table 4 and Fig. 2). All samples presented this decay although to different degrees, more pronounced in M3 samples.

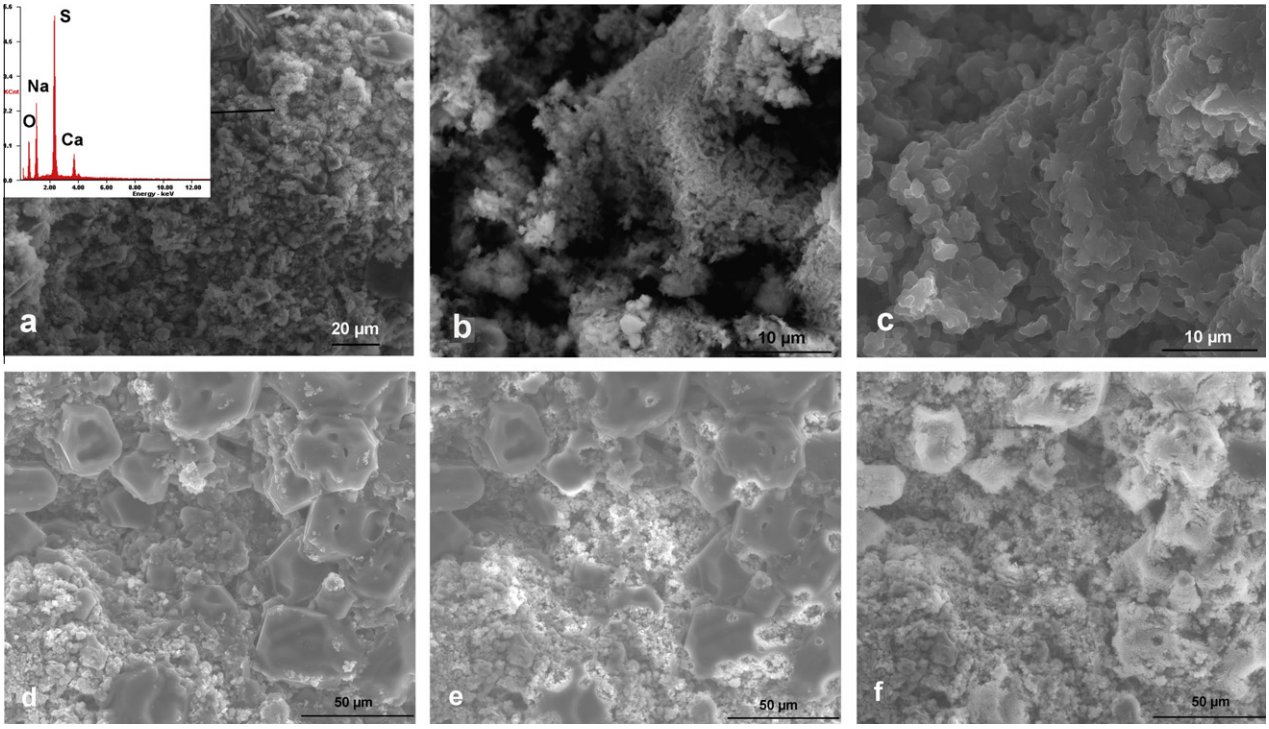

Fig. 9. ESEM images of one of the mortars after the WS + SS test: (a) aspect of the sample at anhydrous conditions (T = 10 °C and RH = 20%). The inset shows the EDX analysis of the salt, indicating that it is a sodium sulphate (thenardite, Na_2SO_4); (b) fibrous morphology of the surface of thenardite crystals at anhydrous conditions; (c) beginning of the hydration and expansion of the thenardite crystals; (d) mirabilite ($Na_2SO_4{\cdot}10H_2O$) crystals with size comprised between 20 and 50 μm, formed at T = 2 °C and RH = 58%; (e) beginning of the dehydration process in some mirabilite crystals, at T = 2 °C and RH = 37.7%; (c) thenardite crystals formed at T = 2 °C and RH = 34.8%.

The salt detected by XRD in mortar samples after WS + SS is thenardite (Na_2SO_4), which is the anhydrous phase of sodium sulphate which precipitates from solution at temperatures higher than 32.4 °C, below which mirabilite is stable ($Na_2SO_4{\cdot}10H_2O$). This means that, during the temperature and humidity cycles established in this study, mirabilite is also present in mortar samples. Ettringite and gypsum have not been detected by means of XRD, although the morphology of cracks (Fig. 4c) developed in mortars may indicate their formation. This can be explained knowing that the decay caused by sodium sulphate is big if thenardite crystals are formed due to heterogeneous nucleation in small fractures or micropores smaller than 1 μm [26]. At the same time, it might be possible that colloidal ettringite has formed in mortars with the highest content of lime [27,50].

From the pore size distribution curves of the altered samples it is clear that a strong reduction in the volume of pores of radius between 0.1 and 1 μm has occurred, and that a new family of pores with radius comprised between 3 and 50 μm has been produced (Fig. 8b). This is because the precipitation of mirabilite from the supersaturated solution, produced at room temperature by the dissolution of thenardite, creates a crystallization pressure [15,51] high enough to break the original pores and generate others with bigger radius.

As found by other authors [52,53], mortar porosity is higher after the absorption of salt (Table 5).

3.3.2. WS + SD

In this test, the absorption of sprayed salt solution by the samples' surface led to a general increase in weight until the 16th cycle in M9 and up to the 22nd for M6; after that, these two mortars lost weight strongly whilst M3 continued to gain weight and M4 remained quite stable until the end of the test (Fig. 1d).

After 30 cycles, the mortar samples did not show any fissures or breaking and the only changes were in their superficial appearance (Fig. 2d).

The salt absorbed by the surface precipitates in form of efflorescences on the upper and side surfaces of samples and in some cases it is followed by spalling (Table 4 and Fig. 5a). In the bigger face a loss of cohesion between the mortar matrix and the sand grains occurs, leading the sample surfaces to become much rougher and less compact (Table 4 and Fig. 5b), especially after the 10 last cycles (Fig. 2d). The biggest consequence of this deterioration was the loss of aggregate grains and binder (i.e. sanding) from the external surfaces of the samples, in a more pronounced way in M9 and M6 samples, which were characterised by notable weight loss (Fig. 1d). As both weight variation (Fig. 1d) and sample appearance (Fig. 2d) indicate, the degree of alteration is inversely proportional to the lime content of mortars, being the highest in M9 and the lowest in M3 and M4. This type of decay is related with the cohesion between mortar sand grains and matrix, which is much poorer in M9, due to the high content of aggregate in this mortar [49].

The total porosity of mortars after the salt deposition test is lower compared to that of unaltered samples. PSD curves of mortars after WS + SD are very similar to those obtained after the rain simulation experiment (WS + R), showing the main peak centered at 0.5 μm and a small peak centered at 4 μm. This type of PSD curve suggests that the original pores have been blocked by the precipitation of salts inside them.

The fact that no cracks or smaller fissures have been generated by salt deposition, indicates that the salt intake from the mortars surface is lower and that precipitation only occurs at superficial level.

3.3.3. Soluble ions

The soluble ions (Fig. 6) determined in mortar samples after the WS + SS test shows that both the sulphate (Fig. 6a) and the sodium (Fig. 6b) content is proportional to the lime content of the original mortars (Ca^{2+}, Fig. 6c). This indicates that the amount of salts is higher in mortars with higher lime contents, for two main reasons:

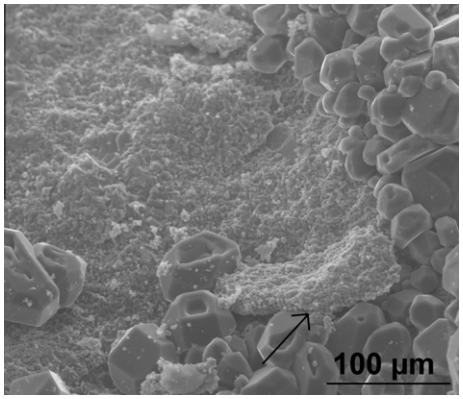

Fig. 10. ESEM image of mirabilite crystals grown within the mortar matrix, which has lost compactness and is progressively pushed by the salt crystals.

on the one hand lime may react with sodium sulphate to form calcium sulphate, so that a higher lime content would produce a higher gypsum content; on the other hand, the porosity of mortars with high lime content is higher and the capillary uptake is more favoured, with the consequence of larger uptake of salts.

After the WS + SD test, a much lower content of sulphates has been found in mortar samples (Fig. 6a) and this agrees with the smaller decay they showed, compared to WS + SS. Nevertheless, a lower correlation has been found between the lime content of the original mortars and the sulphate and sodium content after the test. This is because water uptake does not occur in this test, so that there cannot be a correlation between mortar porosity and superficial decay.

3.3.4. Crystallization at microscopic scale

By means of ESEM, we carried out a dynamic study of the crystallization process at microscopic scale. This allowed us to observe the morphology and size of salt crystals formed at different conditions of temperature and relative humidity. The only salt found in mortars at anhydrous conditions (T = 10 °C and RH = 20%) is thenardite (Fig. 9a and inset), which appeared as fibrous agglomerates (Fig. 9b) with high brightness. The hydration of this phase started at RH = 72.5% when the typical fibres of thenardite (Fig. 10b) started to expand (Fig. 9c) until forming the first mirabilite crystals. The inverse process (dehydration, Figs. 9d–f) started at RH = 37.7% and achieved equilibrium at RH = 34.8%.

Mirabilite crystals precipitated on the surface have sizes between 20 and 50 μm. Even if limited by the size and the pore entrance [16], the maximum crystallization pressure of this salt is still able to overcome the physical constraint of the pore wall (defined by the tensile strength of the material) [15], so that bigger pores of similar size to the mirabilite crystals are generated (Fig. 8b). Moreover, the volume expansion (314% [51]) of the hydrated sodium sulphate is responsible for the big cracks obtained at the end of the WS + SS test in all samples (Table 4, Fig. 2).

By means of the ESEM it was possible to observe how the performance of continuous hydration/dehydration cycles causes the loss of compactness in the matrix (Fig. 10), with a consequent reduction of the sample weight when the salt crystallizes near the surface (as found in M9 after WS + SD, see Fig. 5).

4. Conclusions

This study has shown how differently mortars used to render historic buildings behave according to the mechanism and the agent of attack. It has been found that mortars are much more resistant to salt deposition than to salt capillary uptake because the former only produces superficial decay whilst the latter generates internal cracks.

It has been demonstrated that in mortars with higher contents of binder water uptake is more favoured and drives harmful decay, in the form of spalling, sanding and cracks. In particular, layer detachment can cause a lack of adhesion between the mortar surface and the material (brick, stone) in joints or on the surface. On the other hand, it has been found that the use of high proportions of aggregate can worsen the mortar cohesion, with the main consequence that the mortar suffers a larger amount of superficial decay.

These findings demonstrate, on the one hand, how important is the choice of a correct methodology to determine the durability of construction materials; on the other hand, how controversial is the selection of a good mortar to be used as rendering materials. Both choices must be made considering the decay produced by weathering cycles that most reproduce the climate of the particular location of the historic building as well as the final function of the material in the masonry structure. For example, the salt deposition test (WS + SD) carried out in this study aimed to investigate the superficial decay of mortars caused by the deposition of a salt solution. In this sense, it accurately defines the decay of rendering mortars, whose surface is constantly exposed to external conditions, whilst the salt absorption test (WS + SS) is more representative of the damage caused by capillary rise uptake in ancient buildings where rain accumulation and high phreatic levels occur.

The question that arises is which binder-to-sand ratio is appropriate for a render, whether the one that might give place to slow decay in terms of water/salt solution absorption by capillarity or the one that might be more resistant to the superficial attack of a salt solution.

In our opinion, the surface properties of a render should be preserved as long as possible, especially when this render has an artistic, historic or cultural value. We must not forget that a render is frequently not only the sacrificial layer of a wall, but also the support of a stucco, a wall painting or a similar decoration. In this sense, its aesthetic function has to be preserved. For this reason, we would avoid the use of a mortar with high aggregate proportions because, as seen here, its original superficial appearance appears to become very damaged after weathering.

Among the mortars studied here, we consider that the one with 1:4 binder-to-sand proportion represents the halfway point between two bad extremes. In fact, M4 is the most carbonated mortar and one of the two mortars which presented the lowest superficial decay after salt deposition.

Regarding the methodology proposed in this study, it is fundamental to point out that although the tests have been performed simulating the climatic conditions of the city of Granada, they can certainly be taken as good reference for other Mediterranean areas and those with milder climate, since they cover a wide range of temperature and relative humidity.

Further studies should concentrate on the application of the tests performed in this work on other types of mortars, in order to consider the importance of the variability of the materials (i.e., grain size of the aggregate, proportions of metakaolin, other admixtures).

Acknowledgements

This study was financially supported by Research Group RNM179 of the Junta de Andalucía and by Research Project MAT2008-06799-C03-03. We are grateful to Dr Mona Edwards for her assistance in the programming of the environmental cabinet and the use of the Dionex.

References

[1] Wood C. Understanding and controlling the movement of moisture through solid stone masonry caused by driving rain. MSc Thesis; University of Oxford; 2010.
[2] Hall C, Hoff WD. Rising damp: capillary rise dynamics in walls. Proc Roy Soc 2007;463:1871–84.
[3] Groot C, Gunneweg JTM. The influence of materials characteristics and workmanship on rain penetration in historic fired clay brick masonry. Heron 2010;55(2):141–54.
[4] Groot C. Performance and repair requirements for renders and plasters. RILEM TC203-RHM, ITAM, Prague; 2010.
[5] Rossi-Doria PR. Mortars for restoration: basic requirements and quality control. Mater Struct 1986;19(114):445–8.
[6] Maurenbrecher AHP. Mortars for repair of traditional masonry. ASCE Practice Periodical on Structural Design and Construction; 2004. p. 62–5.
[7] Charola AE. Stone deterioration in historic buildings and monuments. In: proceedings of the 10th international congress on deterioration and conservation of stone, Stockholm; 2004. p. 3–14.
[8] Lanas J, Sirera R, Alvarez JI. Study of the mechanical behaviour of masonry repair lime-based mortars cured and exposed under different conditions. Cem Concr Res 2006;36:961–70.
[9] Cavdar A, Yetgin S. Investigation of mechanical and mineralogical properties of mortars subjected to sulfate. Constr Build Mater 2010;24:2231–42.
[10] Lubelli B, Nijland TG, van Hees RPJ, Hacquerbord A. Effect of mixed in crystallization inhibitor on resistance of lime-cement mortar against NaCl crystallization. Constr Build Mater 2010;24:2466–72.
[11] Karatasios I, Kilikoglou V, Theoulakis P, Colston B, Watt D. Sulphate resistance of lime-based barium mortars. Cem Concr Compos 2008;30:815–21.
[12] Cardell C, Benavente D, Rodríguez-Gordillo J. Weathering of limestone building material by mixed sulfate solutions. Characterization of stone microstructure, reaction products and decay forms. Mater Charact 2008;59:1371–85.
[13] Silva MAG, Silva ZCG, Simao J. Petrographic and mechanical aspects of accelerated ageing of polymeric mortars. Cem Concr Compos 2007;29:146–56.
[14] Cultrone G, Sebastian E, Ortega Huertas M. Durability of masonry systems: a laboratory study. Constr Build Mater 2007;21:40–51.
[15] Steiger M. Crystal growth in porous materials – I: The crystallization pressure of large crystals. J Cryst Growth 2005;282:455–69.
[16] Steiger M. Crystal growth in porous materials – II: Influence of crystal size on the crystallization pressure. J Cryst Growth 2005;282:470–81.
[17] Goudie AS, Wright E, Viles HA. The role of salt (sodium nitrate) and fog in weathering: a laboratory simulation of conditions in the northern Atacama Desert, Chile. Catena 2002;48:255–66.
[18] Rodríguez Navarro C, Doehne E. Salt weathering: influence of evaporation rate, supersaturation and crystallization pattern. Earth Surf Process Land 1999;24:191–209.
[19] Scherer GW. Crystallization in pores. Cem Concr Res 1999;29:1347–58.
[20] Goudie AS, Parker AG. Experimental simulation of rapid rock blosk disintegration by sodium chloride in a foggy coastal desert. J Arid Environ 1998;40:347–55.
[21] Ouyang C, Nanni A, Chang WF. Internal and external sources of sulfate ions in Portland cement mortar: two types of chemical attack. Cem Concr Res 1988;18:699–709.
[22] Tesch V, Middendorf B. Occurrence of thaumasite in gypsum lime mortars for restoration. Cem Concr Res 2006;36:1516–22.
[23] Crammond N. The occurrence of thaumasite in modern construction – a review. Cem Concr Compos 2002;24:393–402.
[24] Benavente D, Garcia del Cura MA, Garcia-Guinea J, Sanchez-Moral S, Ordoñez S. Role of pore structure in salt crystallisation in unsaturated porous stone. J Cryst Growth 2004;260:532–44.
[25] Ruiz-Agudo E, Mees F, Jacobs P, Rodriguez-Navarro C. The role of saline solution properties on porous limestone salt weathering by magnesium and sodium sulphates. Environ Geol 2007;52:269–81.
[26] Rodríguez-Navarro C, Doehne E, Sebastian E. How does sodium sulphate crystallize? Implications for the decay and testing of building materials. Cem Concr Res 2000;30:1527–34.
[27] Cerulli T, Pistolesi C, Maltese C, Salvioni D. Durability of traditional plasters with respect to blast furnace slag-based plaster. Cem Concr Res 2003;33:1375–83.
[28] Horemans B, Cardell C, Bencs L, Kontozova-Deutsch V, De Wael K, Van Grieken R. Evaluation of airborne particles at the Alhambra monument in Granada, Spain. Microchem J 2011;99:429–38.
[29] Lyamani H, Bravo Aranda JA, Alados Arboledas L. Informe de Calidad del Aire de Granada: Año 2009. Grupo de Física de la Atmósfera. Universidad de Granada: Centro Andaluz del Medio Ambiente; 2010.
[30] Cultrone G, Arizzi A, Sebastian E, Rodriguez-Navarro C. Sulfation of calcitic and dolomitic lime mortars in the presence of diesel particulate matter. Environ Geol 2008;56:741–52.
[31] Sabbioni C, Zappia G, Ghedini N, Gobbi G, Favoni O. Black crusts on ancient mortars. Atmos Environ 1998;32:215–23.
[32] Martinez-Ramirez S, Puertas F, Blanco-Varela MT, Thompson GE. Studies on degradation of lime mortars in atmospheric simulation chambers. Cem Concr Res 1997;27(5):777–84.
[33] Zappia G, Sabbioni C, Pauri MG. Mortar damage due to airborne sulphur compounds in a simulation chamber. Mater Struct 1994;27:469–73.
[34] Hossain KMA, Lachemi M, Sahmaran M. Performance of cementitious building renders incorporating natural and industrial pozzolans under aggressive airborne marine salts. Cem Concr Compos 2009;31:358–68.
[35] Ruiz-Agudo E, Lubelli B, Sawdy A, van Hees R, Price C, Rodriguez-Navarro C. An integrated methodology for salt damage assessment and remediation: the case of San Jerónimo Monastery (Granada, Spain). Environ Earth Sci; 2011. doi: 10.1007/s12665-010-0661-9.
[36] Kontozova-Deutscha V, Cardell C, Urosevic M, Ruiz Agudo E, Deutsch F, Van Grieken R. Characterization of indoor and outdoor atmospheric pollutants impacting architectural monuments: the case of San Jerónimo Monastery (Granada, Spain). Environ Earth Sci; 2011. doi: 10.1007/s12665-010-0657-5.
[37] UNE-EN 459-1. Cales para la construcción. Parte 1: Definiciones, especificaciones y criterios de conformidad. AENOR, Madrid; 2002.
[38] ASTM C618-08. Standard Specification for Coal Fly Ash and Raw or Calcined Natural Pozzolan for Use in Concrete. Annual Book of ASTM Standard; 2008 [4.02].
[39] UNE EN 1015-2. Métodos de ensayo de los morteros para albañilería. Parte 2: Toma de muestra total de morteros y preparación de los morteros para ensayo. AENOR, Madrid; 1999.
[40] Cazalla O. Morteros de cal. Aplicación en el Patrimonio Histórico. PhD. Thesis. Universidad de Granada; 2002.
[41] RILEM. Recommended tests to measure the deterioration of stone and to assess the effectiveness of treatment methods (V-1a, V-1b, V-2). Mater Struct 1980;75:175–253.
[42] CEN (), EN 12370. Natural stone test methods—determination of resistance to salt crystallisation. Bruxelles; 1999.
[43] Martín Ramos JD. XPowder. A software package for powder X-ray diffraction analysis. Lgl. Dep. GR 1001/04; 2004.
[44] Moorehead DR. Cementation by the carbonation of hydrated lime. Cem Concr Res 1986;16:700–8.
[45] Matschei T, Lothenbach B, Glasser FP. The role of calcium carbonate in cement hydration. Cem Concr Res 2007;37:551–8.
[46] Cizer O. Competition between carbonation and hydration on the hardening of calcium hydroxide and calcium silicate binders. PhD Thesis. Katholieke Universiteit Leuven; 2009.
[47] Cultrone G, Sebastián E, Ortega Huertas M. Forced and natural carbonation of lime-based mortars with and without additives: mineralogical and textural changes. Cem Concr Res 2005;35:2278–89.
[48] Menéndez E, de Frutos J, Andrade C. Internal deterioration of mortars in freeze–thawing: non-destructive evaluation by means of electrical impedance. Adv Mater Res 2009;68:1–11.
[49] Arizzi A, Martínez-Martínez J, Cultrone G, Benavente D. Mechanical evolution of lime mortars during the carbonation process. Key Eng Mater 2011;465:483–6.
[50] Metha PK. Mechanism of expansion associated with ettringite formation. Cem Concr Res 1976;3:1–6.
[51] Tsui N, Flatt RJ, Scherer GW. Crystallization damage by sodium sulfate. J Cultural Heritage 2003;4:109–15.
[52] Bochen J, Gil S, Szwabowski J. Influence of ageing process on porosity changes of the external plasters. Cem Concr Compos 2005;27:769–75.
[53] Bochen J. Study on the microstructure of thin-layer facade plasters of thermal insulating system during artificial weathering. Constr Build Mater 2009;23:2559–66.